The 9th European Congress on Computational Methods in Applied Sciences and Engineering
ECCOMAS Congress 2024
3–7 June 2024, Lisboa, Portugal

MODELING OF FIBER-REINFORCED, PRESSURISED AND PREFORMED HOSES

QUIRIN HOESCH[1,2], MICHAEL ROLLER[1], FABIO SCHNEIDER-JUNG[1], JOACHIM LINN[1] AND RALF MÜLLER[2]

[1] Fraunhofer Institute for Industrial Mathematics ITWM
Fraunhofer Platz 1, 67663 Kaiserslautern, Germany
e-mail: [quirin.hoesch, michael.roller, fabio.julian.schneider-jung, joachim.linn]@itwm.fraunhofer.de

[2] Technical University of Darmstadt
Franziska-Braun-Straße 7, 64287 Darmstadt, Germany
email: ralf.mueller@mechanik.tu-darmstadt.de

Key words: Hose simulation, Fiber reinforcement, Toroidal helix, Internal pressure, Finite element method

Summary. In this work, we study the effects of fiber reinforcements on the deformation behavior of hoses under internal pressure. We model helically wound reinforcements in three configurations: a straight hose, a full torus and a quarter torus. For straight hoses, the deformation in both diameter and length is significantly influenced by the wrapping angle of the fibers. Notably, a neutral wrapping angle exists where no deformation occurs under internal pressure. For the full and quarter torus models, the variation of the toroidal helix wrapping angle along the cross-section is taken into account. We discuss the extent to which the type and orientation of the fiber reinforcements affect the Bourdon effect, using the finite element method.

1 INTRODUCTION

Hoses are mainly made of fiber-reinforced rubber, with reinforcements varying from nylon to steel. The application fields range from the automotive, heavy and agricultural machinery industry to rail vehicle technology. There they perform important functions, e.g. as brake hoses, coolant hoses, air intake hoses or fuel hoses, where their use is particularly advantageous in scenarios where rigid pipes are impractical due to considerations of weight, assembly complexity or the necessity for flexible connection points. In this context, interactive assembly simulations for flexible structures, such as cables and hoses, play a crucial role in vehicle development [1, 2]. These simulations commonly utilize geometrically non-linear rod models [3]. However, when the hoses are curved, fiber-reinforced and pressurised, deformation behavior occurs that cannot be easily predicted using nonlinear rod theory. A 3D continuum model is used to evaluate how curvature, helical reinforcement and internal pressure affect the hose deformation. In our current work, we focus on the influence of a single reinforcement layer on the deformation behavior. For straight hoses, the deformation in diameter and length due to the internal pressure depends on the wrapping angle of the fibers. The effect of the neutral angle in hydraulic hoses, in literature sometimes also called critical angle at which the hose doesn't deform, has been studied based on

membrane theory in [4, 5], on classical laminate shell theory in [6, 7] and on three-dimensional elastic theory in [8, 9, 10]. Experimental change-in-length tests for manufacturers of high-pressure hydraulic hoses are described in [11]. This standard provides detailed instructions for conducting the experiments and outlines the acceptable elongation or shortening limits based on the hose's construction and size. The mechanical behavior of curved, linear-elastic and isotropic structures under internal pressure has been studied in [12, 13]. The so-called Bourdon effect describes how internal pressure in a curved hose generates an outward resultant force that tends to straighten the bend, thereby increasing deformations and stress levels. An analytical description of the varying wrapping angle of a toroidal helix along the cross-section of curved structures is provided in [14]. For the procedure of winding on the curved parts of a composite frame, a mathematical model, which describes how to determine the number of rovings on toroidal parts is presented in [15]. The structure of this paper is as follows: Section 2 presents an analytical examination of the neutral wrapping angle in straight hoses, the Bourdon effect and the variation of the wrapping angle of a toroidal helix. Section 3 details the structure and model parameters employed in our finite element analysis. Section 4 shows the numerical results for the examples of a straight hose, a full torus and a quarter torus and discusses the characteristics that influence the Bourdon effect. Section 5 offers concluding remarks.

2 THEORETICAL BACKGROUND

In this section, we present analytical considerations which are relevant for the description of the behavior of reinforced, curved hoses. We give a brief introduction to the already known neutral wrapping angle of straight hoses. We extend this to curved hoses by presenting the Bourdon effect. Finally, we combine the curved hose with the helically reinforcement by deriving the varying wrapping angle of the toroidal helix.

2.1 Neutral angle

In the study of reinforced straight hoses under internal pressure, the concept of the neutral wrapping angle plays a crucial role. This angle, at which the reinforcing fibers are wound helically around the hose, is essential in balancing the internal stresses induced by the pressure. The internal forces are counterbalanced by the helical reinforcement, preventing any elongation or contraction of the hose and maintaining its structural integrity and functionality. In the following, we derive the expression for the neutral wrapping angle γ_N.

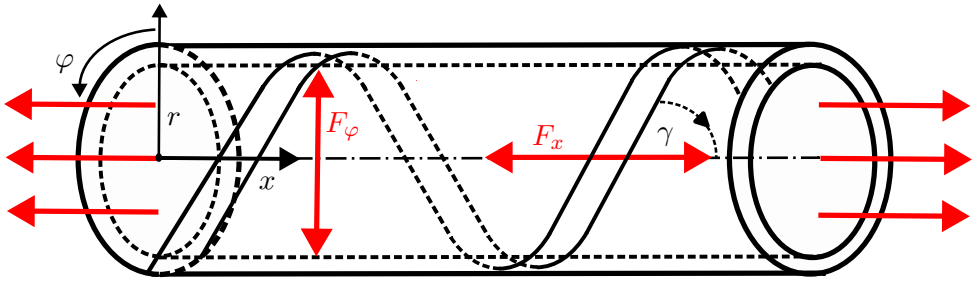

Figure 1: Forces acting on a reinforced hose under internal pressure

We consider the hose as a straight cylinder closed at both ends with the radius r, the length L and a wrapping angle γ, see Fig. 1. We use a cylindrical coordinate system with the directions r-radial, φ-hoop and x-axial. The following analytical considerations are based on thin-walled membrane theory, so that the normal stress in the radial direction σ_r can be neglected, assuming a plane stress state. The principal stresses here are as follows

$$\boldsymbol{\sigma} = \begin{pmatrix} \sigma_1 & 0 \\ 0 & \sigma_2 \end{pmatrix} = \begin{pmatrix} \sigma_\varphi & 0 \\ 0 & \sigma_x \end{pmatrix}; \quad \text{with} \quad \sigma_\varphi = \frac{pr}{h}, \quad \sigma_x = \frac{pr}{2h}. \tag{1}$$

The angle γ_R of the resultant force F_φ and F_x (see Fig. 1) can be expressed by

$$\tan\gamma_R = \frac{F_\varphi}{F_x} = \frac{prL}{p\pi r^2} = \frac{L}{\pi r}. \tag{2}$$

The length of one helix turn is given by

$$L = \frac{2\pi r}{tan\gamma}. \tag{3}$$

For equilibrium state, the helix angle γ should correspond to the angle of the resultant force γ_R, so that $\gamma = \gamma_R$. By inserting (3) in (2) we get the angle γ_N at which no deformation occurs when the hose is pressurised:

$$\tan\gamma_R = \frac{2}{\tan\gamma} = \tan\gamma \quad \rightarrow \quad \gamma_N = \tan^{-1}(\sqrt{2}) = 54.74°. \tag{4}$$

.

2.2 Bourdon effect

Internal pressure in curved hoses generates an outward force that causes the hose to straighten. This effect is known as the Bourdon effect [16]. For the modeling of structures with a curved center line, a toroidal coordinate system is used with the three coordinate directions r - radial, θ - toroidal and φ - poloidal. The poloidal angle $\varphi = \frac{\pi}{2}$ is called extrados, $\varphi = \frac{3\pi}{2}$ is called intrados, while $\varphi = 0 = \pi$ is called crown, see Fig. 2.

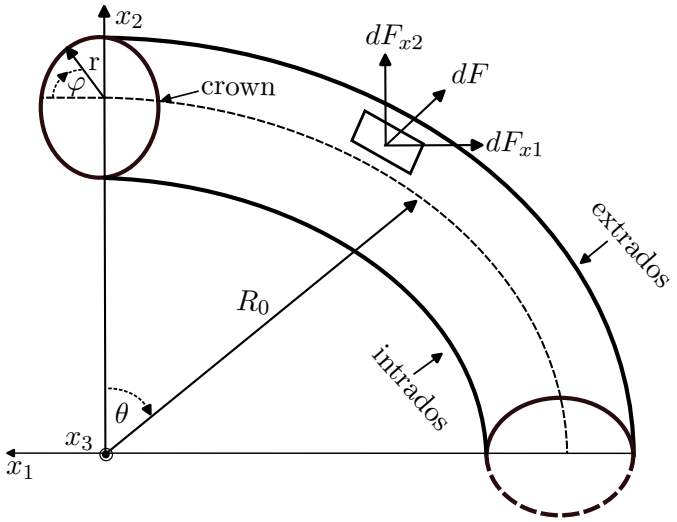

Figure 2: Outwardly directed force on an infinitesimal area dA of a pressurised curved hose

To analyze the Bourdon effect in a pressurised toroidal structure, we determine the effective outward force $\vec{F}$ by integrating the pressure p over an infinitesimal area dA. The area dA of a torus can be described as follows

$$dA = r(R_0 + r\sin\varphi)d\varphi d\theta. \tag{5}$$

The outwardly directed force $\vec{F}$ can be decomposed then into the components F_{x1} and F_{x2}

$$F_{x1} = -\int_{\theta_1}^{\theta_2} p\pi r^2 \sin\theta d\theta, \qquad F_{x2} = \int_{\theta_1}^{\theta_2} p\pi r^2 \cos\theta d\theta. \tag{6}$$

The force component F_{x3} disappears when being integrated along the cross-section φ, so that no Bourdon force appears in the x_3-direction. A more detailed description of the derivation of the infinitesimal area dA and the Bourdon forces F_{x1} and F_{x2} can be found in [17, 18].

2.3 Toroidal helix

In Fig. 3a, a straight helix is shown to introduce relevant parameters for helical structures. The wrapping angle γ describes the angle of the helix to the neutral fiber. The helix angle α is the complementary value ($\alpha = \frac{\pi}{2}$ - γ), describing the angle between the helix and his base area. The pitch h describes the vertical distance between two consecutive turns ($h = 2\pi r \tan\alpha$), while N characterizes the number of turns, so that the length of the neutral fiber is given by $L = Nh$. For helically fiber reinforced curved structures, a helical pattern is wrapped around a torus, hereafter called toroidal helix, see Fig. 3b. We therefore take into account that, unlike in a straight helix, the wrapping angle of a toroidal helix is not uniform, but varies along the cross-section of the torus. We remain in the toroidal coordinate system defined in Section 2.2, so that the parametrization of a toroidal helix is as follows

$$\begin{aligned} x_1(\varphi,\theta) &= (R_0 + r\sin(N\varphi))\cos\theta, \\ x_2(\varphi,\theta) &= (R_0 + r\sin(N\varphi))\sin\theta, \\ x_3(\varphi,\theta) &= -r\cos(N\varphi). \end{aligned} \tag{7}$$

The tangent vector $\vec{t}$ at any point of the toroidal helix can be obtained by the following procedure. First we form in (8) the partial derivatives of the Cartesian coordinates x_1, x_2 and x_3 according to the angular coordinates of the torus θ and φ, then we determine in (10) the change in arc length ds using the infinitesimal Cartesian changes dx_1, dx_2 and dx_3 of (9).

$$\begin{aligned} \frac{\partial x_1}{\partial\varphi} &= rN\cos(N\varphi)\cos\theta, & \frac{\partial x_1}{\partial\theta} &= -(R_0 + r\sin(N\varphi))\sin\theta, \\ \frac{\partial x_2}{\partial\varphi} &= rN\cos(N\varphi)\sin\theta, & \frac{\partial x_2}{\partial\theta} &= (R_0 + r\sin(N\varphi))\cos\theta, \\ \frac{\partial x_3}{\partial\varphi} &= rN\sin(N\varphi), & \frac{\partial x_3}{\partial\theta} &= 0. \end{aligned} \tag{8}$$

$$\begin{aligned} dx_1 &= \frac{\partial x}{\partial\varphi}d\varphi + \frac{\partial x}{\partial\theta}d\theta = (rN\cos(N\varphi)\cos\theta)\,d\varphi - (R_0 + r\sin(N\varphi))\sin\theta\,d\theta, \\ dx_2 &= \frac{\partial x}{\partial\varphi}d\varphi + \frac{\partial x}{\partial\theta}d\theta = (rN\cos(N\varphi)\sin\theta)\,d\varphi + (R_0 + r\sin(N\varphi))\cos\theta\,d\theta, \\ dx_3 &= \frac{\partial x}{\partial\varphi}d\varphi + \frac{\partial x}{\partial\theta}d\theta = rN\sin(N\varphi)d\varphi. \end{aligned} \tag{9}$$

$$ds = \sqrt{dx_1^2 + dx_2^2 + dx_3^2} = \sqrt{(r^2 N^2 d\varphi)^2 + \left((R_0 + r\sin(N\varphi))^2\, d\theta^2\right)}. \tag{10}$$

$$\vec{t} = \left(\frac{dx_1}{ds},\ \frac{dx_2}{ds},\ \frac{dx_3}{ds}\right)^T. \tag{11}$$

The tangent vector $\vec{u}$ of the neutral fiber of the torus can be expressed using the unit circle

$$\vec{u} = (-\sin\theta,\ \cos\theta,\ 0)^T. \tag{12}$$

By using the scalar product between the tangent vector of the toroidal helix $\vec{t}$ and the tangent vector of the unit circle $\vec{u}$, the wrapping angle γ of the toroidal helix around the torus is calculated including the simplification of trigonometric functions due to periodicity

$$cos\gamma = \vec{t}\cdot\vec{u} \quad \rightarrow \quad \gamma = \cos^{-1}\left(\frac{R_0 + r\sin\varphi}{\sqrt{r^2N^2 + (R_0 + r\sin\varphi)^2}}\right). \tag{13}$$

The wrapping angle γ varies along the torus, showing that the angle is smaller at the extrados of the torus ($\varphi = \frac{\pi}{2}$) and larger at the intrados ($\varphi = \frac{3\pi}{2}$), see the black line in Fig. 3c. On the crown ($\varphi = 0, \pi$), the wrapping angle γ corresponds to the one of a straight helix, when the number of windings N and the length of the neutral axis L for a toroidal and straight helix is equal. In the limit range of small curvature, γ becomes approximately constant. For larger curvatures, the variation of the wrapping angle increases. In comparison to a straight helix with constant slope and constant infinitesimal arc length ds, the toroidal helix has a continuous change of the direction of the tangent vector $\vec{t}$, due to a change of the local curvature. Thus, there are differences in the paths of the discretization points on the helix, when it wraps around a torus, which leads to a variable ds, see the red line in Fig. 3c. When the infinitesimal arc length ds increases, the wrapping angle γ decreases and vice versa.

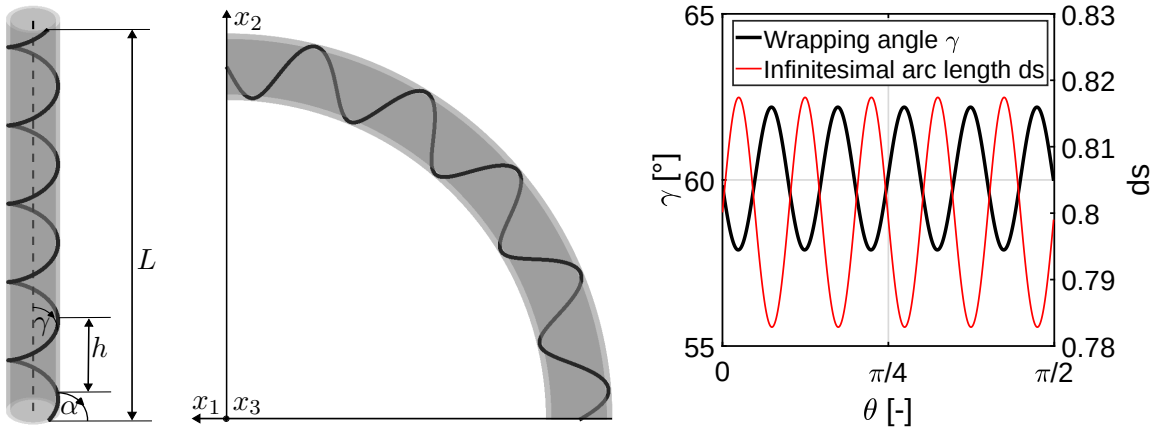

(a) (b) (c)

Figure 3: $N = 5$, $r = 11$, $\gamma_{straight,crown} = 60°$ for straight helix in (a) and toroidal helix in (b). Varying wrapping angle γ of the toroidal helix in (c)

3 FINITE ELEMENT METHOD

For investigating to what extend the type and orientation of the fiber reinforcements affect the deformation behavior of hoses under internal pressure, we use the finite element method with the commercial software ANSYS and its command language APDL [19],[20]. The model parameters are listed in Table 1.

Table 1: Model parameters for finite element analysis

Curvature Radius	Inner Radius	Thickness	Matrix Modulus	Fiber Modulus
R_0	r_i	h	E_M	E_F
$50mm$	$10mm$	$2mm$	$250\frac{N}{mm^2}$	$250{\cdot}10^2\frac{N}{mm^2}$
Poisson's Ratio Matrix	Poisson's Ratio Fiber	Pressure	Volume Ratio Matrix	Volume Ratio Fiber
ν_M	ν_F	p	V_M	V_F
0.4	0.4	$1\frac{N}{mm^2}$	0.75	0.25

Hexahedral 3D continuum elements with 20 nodes are used in this study. Since we want to investigate the influence of a single reinforcement layer, the following examples of a straight hose, a full torus and a quarter torus are discretized with one element in the radial direction, one element per 10° in the circumferential/poloidal direction and a total of 50 elements in the axial/toroidal direction, as illustrated in Fig. 4. In order to consider reinforcements with a reasonable computational effort, we use a smeared modeling approach. This approach is particularly suitable for structures in which the reinforcements are distributed and arranged in an uniform pattern. By integrating the stiffness of the reinforcements into the volumetric elements, we introduce an orthotropy that is aligned with the direction of the reinforcements, specified by the wrapping angle γ. The effective constitutive tensor $\mathbf{C}$ is calculated as the weighted sum of the constitutive tensors of the matrix and the fibers

$$\mathbf{C} = V_M \mathbf{C}_M + V_F \mathbf{C}_F. \tag{14}$$

The analysis is carried out using the theory of large deformations. The internal pressure p is modeled as a follower load in ten load steps. For the quasi-static analysis, the Newton-Raphson algorithm is used, which provides a robust method for solving non-linear equations.

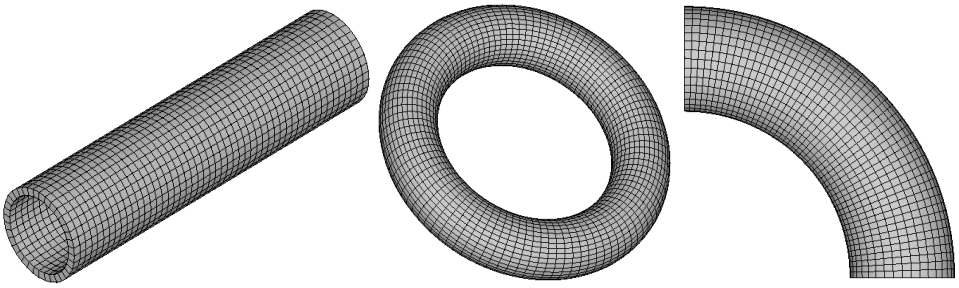

Figure 4: Discretized structure: straight hose, full torus and quarter torus

4 RESULTS AND DISCUSSION

This chapter presents the simulation results for a straight hose, a full torus, and a quarter torus, using the parameters from Chapter 3. It discusses the impact of the fiber orientation on the deformation. In Chapters 4.2 and 4.3, the displayed wrapping angle γ refers to the angle on the crown, with the understanding that it varies along the cross-section, see Section 2.3.

4.1 Straight hose

A partial section of the reinforcement layer of a straight hose is illustrated for the neutral wrapping angle γ_N in Fig. 5a. Fixed-free boundary conditions are applied, with all nodes at $x = 0$ constrained in the way $u^* = u_{x,\varphi} = 0$. Internal pressure is applied to the hose's inner walls and nodal forces at the free end ($x = L$) are added to account for end forces

$$F_{Nodal,End} = \frac{p\pi r_i^2}{n_{Nodal,End}}. \tag{15}$$

Fig. 5b illustrates how the geometry of reinforced hoses is affected by internal pressure loading increase. For the neutral wrapping angle $\gamma_N = 54.74°$ (see solid vertical line), there is no change in the hose geometry, neither in the axial direction x, nor in the radial direction r. For the case $\gamma < \gamma_N$, the hose length decreases with the strain ϵ_x (see solid lines) and the hose diameter increases with the strain ϵ_r (see dashed lines). For the case $\gamma > \gamma_N$, the length of the hose increases, while the hose diameter decreases. The fibers align according to the resulting force due to the internal pressure. The larger the radius of the hose, the greater the change in elongation and contraction in the axial and radial direction.

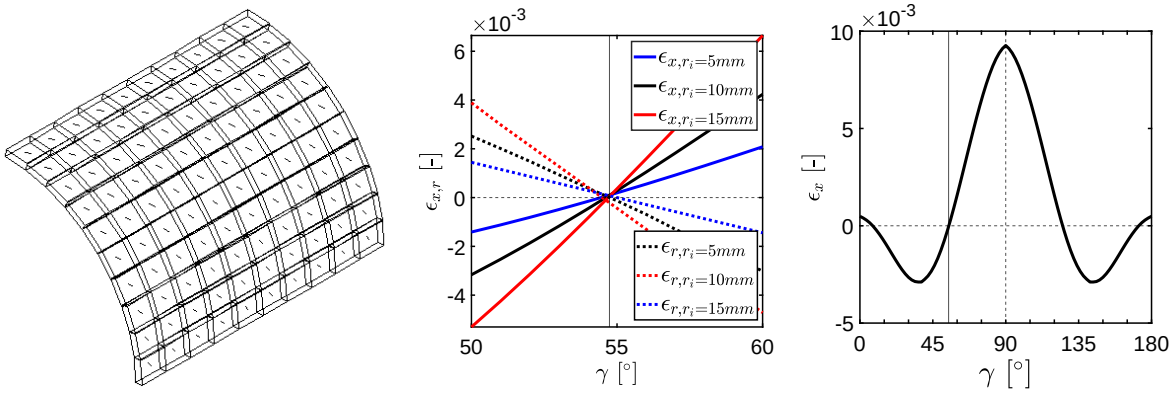

(a) Reinforcement layer for the neutral wrapping angle γ_N

(b) Deformation behavior and neutral wrapping angle γ_N

(c) Axial strain ϵ_x for different wrapping angles γ

Figure 5: Straight hose

Fig. 5c shows the axial deformation behavior with wrapping angles γ varying from 0° to 180°. It demonstrates that the linear relationship from Fig. 5b between the wrapping angle γ and the deformation $\epsilon_{x,r}$ only applies to the range of angles around the neutral wrapping angle γ_N. The deformation curve in Fig. 5c exhibits axial symmetry about the 90° axis (see dashed vertical line), indicating that the axial deformation is independent of the helical winding

direction (whether right-handed or left-handed), due to the zero Gaussian curvature κ along the cross-section. As the wrapping angle γ increases from 0° (fibers parallel to the hose axis), the axial reinforcing effect of the fibers decreases until a certain minimum. The angle at which this minimum occurs, depends on the geometry parameters L and r_i. Beyond, the axial stiffness increases as the fiber orientation becomes more balanced between the circumferential and axial load, until the neutral wrapping angle γ_N is reached. Moving further from γ_N, the stiffness decreases again, reaching an elongation maximum at 90° (fibers form rings around the axis).

4.2 Full torus

For an isotropic full torus, the Bourdon effect uniformly increases the curvature radius R_0. Unlike a straight hose, where a constant neutral wrapping angle γ_N can be theoretically defined (see Section 2.1), such a constant neutral angle does not exist for the torus, due to its varying Gaussian curvature κ. The Gaussian curvature κ varies between negative values (concave area), zero (equatorial line) and positive values (convex area). Boundary conditions are specified along the three symmetry planes of the torus: the horizontal plane and the two vertical planes at $\varphi = \frac{\pi}{2}, \frac{3\pi}{2}$ in the way $u^* = u_\varphi = 0$ and at $\theta = \frac{k\pi}{2}$ (where $k = 0, 1, 2, 3$) in the way $u^* = u_\theta = 0$. In Fig. 6 we have a look at the larger radius of the torus R_0. We present the percentage change of the radius of curvature R_0 for different wrapping angles γ. The torus axes from $\theta = 0 \rightarrow \pi$ is shown in black and from $\theta = \frac{\pi}{2} \rightarrow \frac{3\pi}{2}$ in red. We distinguish between a constant radius of curvature R_0 (solid lines) and a constant number of turns $N \in \mathbb{N}$ (dashed lines). Both are related by the following equation

$$R_0 = Nr \tan\alpha = Nr \tan(\frac{\pi}{2} - \gamma) = Nr \cot(\gamma). \tag{16}$$

For a constant R_0, increasing the wrapping angle γ leads to an increase in the number of turns N, while keeping N constant results in a decrease in R_0 as γ increases. The dashed lines (N_{const}) are not applicable for $\gamma = 0$, $\frac{\pi}{2}$, π, as no toroidal helix exists for these angles. Due to the fiber-induced anisotropy, the expansion of R_0 is uneven, making the torus oval-shaped.

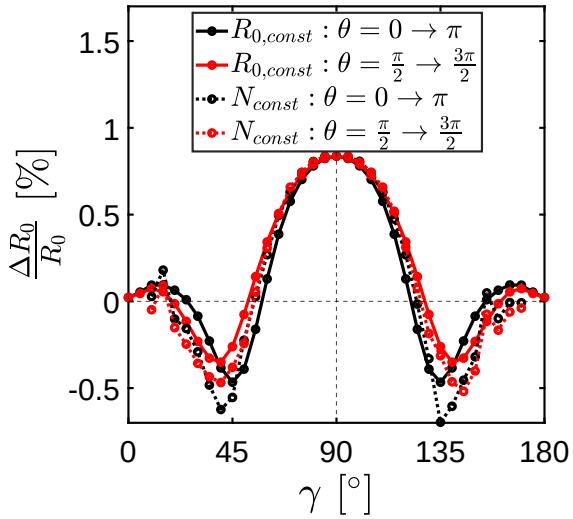

Figure 6: Bourdon effect for a reinforced full torus with $R_0, const = 50$mm and $N_{const} = 8$. Mean value $\frac{\Delta R_0}{R_0} = 0.17\%$

For low and high wrapping angles γ, R_0 even decreases, although the average percentage change $\frac{\Delta R_0}{R_0}$ remains positive, demonstrating the Bourdon effect. A zero-crossing near the neutral wrapping angle γ_N of a straight hose (54.7°) shows that at this angle, the torus experiences no deformation, with neither R_0 nor the arc length changing. In summary, Fig. 6 highlights that the percentage change in the curvature radius (Bourdon effect) depends more on the reinforcement orientation than on the torus geometry. Fig. 7 examines the small radius r of the torus by observing its cross-sectional ovalization. In isotropic tori, ovality arises due to unevenly distributed poloidal stress, with maximum stress at the intrados and minimum stress at the extrados [17]. The ovality is calculated with the main axis a_1 running from extrados to intrados and the main axis a_2 running from crown to crown, as shown in Fig. 2

$$\Omega\ [\%] = \frac{a_1 - a_2}{a_1 + a_2}. \tag{17}$$

We see that the degree of ovalization, whether longitudinal (positive) or transversal (negative), is strongly influenced by the reinforcement orientation, reflecting the material's anisotropy. Fig. 7a shows the ovalization behavior at four toroidal positions for different wrapping angles γ with a constant curvature radius R_0. Due to the anisotropic behavior of a reinforced full torus, the ovalization varies along the toroidal direction θ. While the ovalization along one axis (in this example $\theta = \frac{\pi}{2} \rightarrow \frac{3\pi}{2}$) remain equal, those along the other axis (in this example $\theta = 0 \rightarrow \pi$) differ. Changing the winding direction from left to right-handed, mirrors the deformations along the torus's symmetry planes. This symmetry is evident, as the red line in the $[0°, 90°]$ interval mirrors the black line in the $[90°, 180°]$ interval, and conversely. Besides the wrapping angle γ, the fiber-to-matrix volume ratio also significantly impacts the torus's cross-sectional ovalization. Fig. 7b focuses on the ovalization for right-handed reinforcements (0 to 90°), as the results can be extrapolated to left-handed fibers (90 to 180°) based on the observations from Fig. 7a. The higher the fiber volume ratio, the stronger the ovalization and the influence of the fibers.

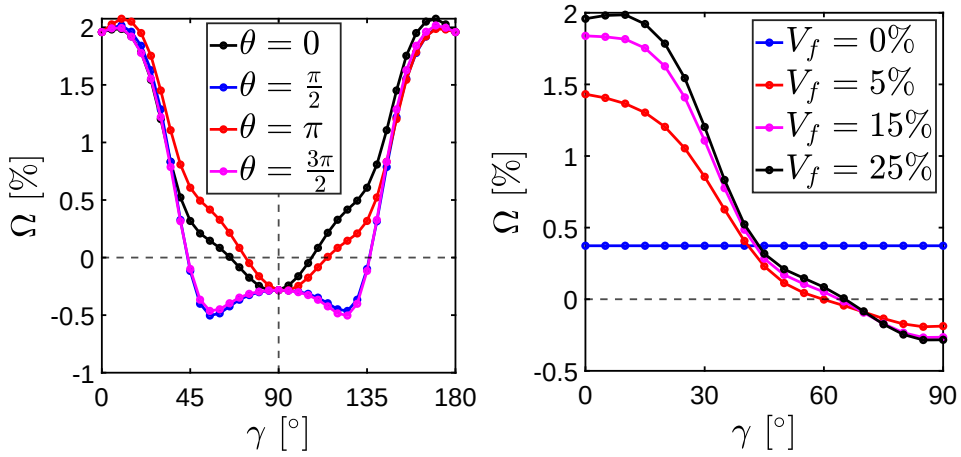

(a) Ovality Ω along a torus for varied wrapping angles γ with $R_{0,const}$

(b) Ovality Ω at $\theta = 0$ for varied fiber volume fractios V_F and wrapping angles γ with $R_{0,const}$

Figure 7: Cross-sectional ovalization behavior in a fiber reinforced full torus

4.3 Quarter torus

The structural response of a pressurised, reinforced quarter torus is shown, using fixed-free boundary conditions. Here, all nodes at $\theta = 0$ are constrained in the way $u^* = u_{\theta,\varphi} = 0$. The Bourdon effect causes the quarter torus to straighten under internal pressure. Thereby, the cross-section remains perpendicular to the toroidal axis, but rotating out of the cross-sectional plane. Fig. 8a illustrates the normalized displacement of the center of gravity at the free end for different wrapping angles γ. The straightening is characterized by x_2 (vertical) and x_1 (horizontal), which are 90° axisymmetric and therefore independent of the winding direction. The deformation in x_3-direction (along the larger axis of rotation) is point-symmetric and therefore dependent of the winding direction, whether right-handed or left-handed. Consequently, the direction of bending during the fabrication of curved fiber-reinforced hoses has an impact on their deformation direction, an aspect that has not been adequately addressed in the existing literature. Fig. 8b shows the vertical displacement of the center of gravity $\Delta x_{2,S}$ against different wrapping angles γ for $R_0 = \text{const.}$ and $N = \text{const.}$ Here again, for $N = \text{const.}$, no toroidal helix exist at $\gamma = 0$, $\frac{\pi}{2}$ and π. As in Section 4.2, a small γ results in a high curvature radius R_0, showing that the normalized straightening of a quarter torus $\frac{\Delta x_{2,S}}{R_0}$ with unsymmetrical boundary conditions depends more on the geometry than on the reinforcement orientation.

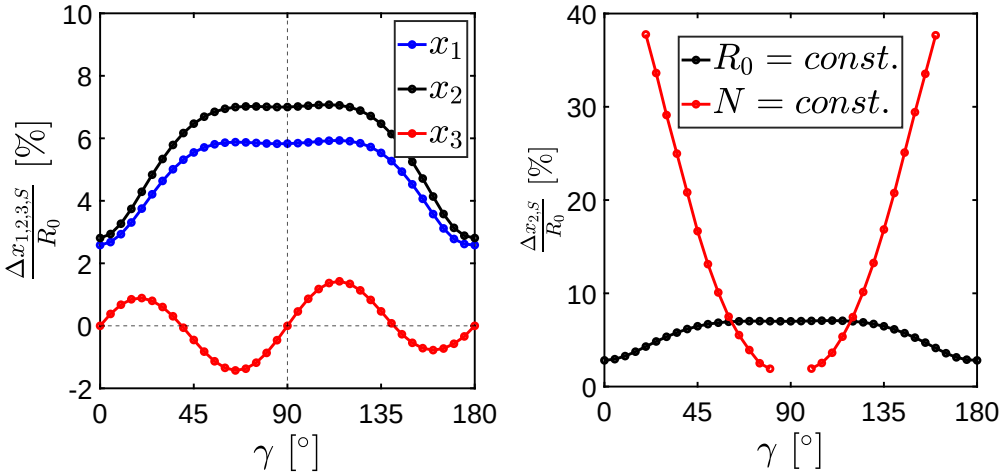

(a) Deformation of the free end for varied wrapping angles γ with $R_{0,const}$

(b) Comparison of the straightening between $R_{0,const} = 50\text{mm}$ and $N_{const} = 2$

Figure 8: Bourdon effect for a quarter torus

5 CONCLUSION AND OUTLOOK

This study has examined the deformation behavior of fiber-reinforced hoses under internal pressure, focusing on both straight and curved configurations. In curved, pressurised structures, the Bourdon effect emerges as the most significant factor influencing the deformation. For a full torus, the deformation behavior of the larger circle (radius R_0) and the ovalization of the smaller circle (radius r), are primarily governed by the wrapping angle γ, with less dependence on the geometry R_0. Conversely, in the quarter torus, the deformation is predominantly influenced

by the geometry R_0, with less impact from the wrapping angle γ, due to the asymmetrical boundary conditions applied. As a result, the deformation along the axis of rotation depends on the winding direction (right-handed or left-handed). Furthermore, for a full torus, there exists a varying wrapping angle γ, at which no curvature radius expansion ΔR_0 takes place, analogous to the neutral wrapping angle γ_N of a straight hose. This concept of the neutral wrapping angle γ_N, originally defined for straight hoses, can be adapted to toroidal geometries. In this context, reinforcement fibers should be aligned with the torus's geodesics - the shortest paths along its surface, typically following spiral trajectories. Aligning the reinforcement with these geodesic paths can achieve an isotensoidal load distribution, where the load is evenly distributed across the toroidal surface, allowing the reinforcements to counterbalance internal forces, thereby preventing any elongation or contraction of the torus. Future research could investigate the extension of the single reinforcement layer to multiple layers to analyze how the positioning of these layers within the cross-section affects the deformation behavior. In this context, the feasibility of reducing the 3D continuum model to a shell model could be investigated. However, it must be ensured that the deformation behavior and all relevant effects are accurately captured. This reduction is particularly relevant for composite materials, where the complex interactions between multiple layers and the anisotropic properties can be effectively taken into account.

REFERENCES

[1] Linn, J., Schneider, F., Dreßler, K. and Hermanns, O. Virtual Product Development and Digital Validation in Automotive Industry. *In: Bock, H.G., Küfer, KH., Maass, P., Milde, A., Schulz, V. (eds): German Success Stories in Industrial Mathematics.* Mathematics in Industry (2021), vol **35**, pp.45-52. Springer, Cham.

[2] IPS Cable Simulation Software. *https://flexstructures.com*

[3] Linn, J., Hermansson, T., Andersson, F. and Schneider, F. Kinetic aspects of the discrete Cosserat rods based on the difference geometry of framed curves. *Proceedings of the 8th ECCOMAS Thematic Conference on Multibody Dynamics* (2017), pp.163-175, Prague.

[4] Van den Horn, B. and Kuipers, M. Strength and Stiffness of a reinforced flexible hose. *Applied Scientific Research* (1988), vol **45**(3), pp.251-281.

[5] Entwistle, K. and White, G. A method for archieving load transfer between the inner and outer layers of a two-layer braided high-pressure hydraulic hose. *International Journal of Mechanical Sciences* (1977), vol **19**(4), pp.193-201.

[6] Zhou, Y., Duan, M., Ma, J. and Sun, G. Theoretical analysis of reinforcement layers in bonded flexible marine hose under internal pressure. *Engineering Structures* (2018), vol **168**, pp.384-398.

[7] Geng, P., Xing, J. Z. and Chen, X. X. Winding angle optimization of filament-wound cylindrical vessel under internal pressure. *Archive of Applied Mechanics* (2016), vol. **87**, pp.365–384.

[8] Bai, Y., Chen, W., Xiong, H., Qiao, H. and Yan, H. Analysis of steel strip reinforced thermoplastic pipe under internal pressure. *Ships and Offshore Structures* (2015), vol **11**, pp.766-773.

[9] Xia, M., Takayanagi, H. and Kemmochi, K. Analysis of multi-layered filament-wound composite pipes under internal pressure. *Composite Structures* (2001), vol **53**, pp.483-491.

[10] Xing, J., Geng, P. and Yang, T. Stress and deformation of multiple winding angle hybrid filament-wound thick cylinder under axial loading and internal and external pressure. *Composite Structures* 2015, vol **131**, pp.868-877.

[11] ISO 6605. Hydraulic fluid power — Hoses and hose assemblies — Test methods. *International Organization for Standardization*, 2002.

[12] Abdulhameed, S., Adeeb, R., Cheng, R. and Martens, M. The Influence of the Bourdon Effect on Pipe Elbow. *Proceedings of the 11th International Pipeline Conference* (2016), Calgary, Alberta, Canada, IPC2016-64659. https://doi.org/10.1115/IPC2016-64659.

[13] Shemirani, F., Adeeb, S., Cheng R. and Martens, M. Investigation of the Influence of the Bourdon Effect on the Stress and Ovalization in Elbows. *Proceedings of the 10th International Pipeline Conference* (2014), Calgary, Alberta, Canada, IPC2014-33651. https://doi.org/10.1115/IPC2014-33651.

[14] Bohr, J., Olsen, K.. Geometry of the toroidal N-helix: optimal-packing and zero-twist. *New Journal of Physics* 2012, vol **14(2)**, 023063.

[15] Mlynek, J., Rahimian Koloor, S.S. and Knobloch, R. Optimal Roving Winding on Toroidal Parts of Composite Frames, *Polymers* 2023, vol **15(15)**, 3227.

[16] Bourdon, B., Notes on Pressure Gauges, (1849).

[17] To appear: Hoesch, Q., Roller, M., Schneider-Jung, F., Linn, J. and Müller, R. Analysis and simulation of curved hoses under internal pressure - 3D continuum model. *Proceedings in Applied Mathematics and Mechanics* (2024), Magdeburg. DOI: 10.1002/pamm.2024.00112.

[18] Thiagajaran, N. Estimation of Pipe Elbow Anchor Loads Due to Internal Pressure, *International Journal of Engineering and Innovative Technology* 2013, vol **2**, pp. 314-317.

[19] Zienciewicz, O.C., Taylor, R.L. and Fox, D.D. 2013. The Finite Element Method for Solid & Structural Mechanics, 7th ed. Oxford, Butterworth-Heinemann.

[20] ANSYS Inc. Academic Research Mechanical, Release 24.1.